Uncertainty of stationary and nonstationary models for rainfall frequency analysis

T.B.M.J. Ouarda[1,*], C. Charron[1] and A. St-Hilaire[1]

[1]Canada Research Chair in Statistical Hydro-climatology, INRS-ETE, 490 de la Couronne, Quebec City (QC), G1K9A9, Canada

*Corresponding author:

Email: taha.ouarda@ete.inrs.ca

Tel: +1 418 654 3842

July 2019

Abstract

The development of nonstationary frequency analysis models is gaining popularity in the field of hydro-climatology. Such models account for nonstationarities related to climate change and climate variability but at the price of added complexity. It has been debated if such models are worth developing considering the increase in uncertainty inherent to more complex models. However, the uncertainty associated to nonstationary models is rarely studied. The objective of this paper is to compare the uncertainties in stationary and nonstationary models based on objective criteria. The study is based on observed rainfall data in the United Arab Emirates (UAE) where strong nonstationarities were observed. In this study, a nonstationary frequency analysis introducing covariates into the distribution parameters was carried out for total and maximum annual rainfalls observed in the UAE. The Generalized Extreme Value (GEV) distribution was used to model annual maximum rainfalls and the gamma (G) distribution was used to model total annual rainfalls. A number of nonstationary models, using time and climate indices as covariates, were developed and compared to classical stationary frequency analysis models. Two climate oscillation patterns having strong impacts on precipitation in the UAE were selected: the Oceanic Niño Index and the Northern Oscillation Index. Results indicate that the inclusion of a climate oscillation index generally improves the fit of the models to the observed data and the inclusion of two covariates generally provides the overall best fits. Uncertainties of estimated quantiles were assessed with confidence intervals computed with the parametric bootstrap method. Results show that for the small sample sizes in this study, the width of the confidence intervals can be very large for extreme nonexceedance probabilities and for the most extreme values of the climate index covariates. The weaknesses of nonstationary models revealed by the bootstrap uncertainties are discussed and words of caution are formulated.

Keywords

Rainfall; Arid-climate; Nonstationary frequency analysis; Teleconnection; Climate oscillation index; parametric bootstrap; uncertainty; United Arab Emirates.

1. Introduction

The presence of nonstationarity in hydro-climatic time series in a context of climate change is commonly accepted. Also, large scale oscillation phenomena modulate climate around the world and impact hydro-climatic variables. In classical frequency analysis models, observations are assumed to be independent and identically distributed (*iid*). However, these assumptions are not met in the presence of the nonstationarities. Considerable efforts have hence been invested on the development of nonstationary frequency analysis models for hydro-climatic variables.

One approach frequently used to deal with nonstationarities in data samples is to introduce covariates into the parameters of the distribution (e.g. Strupczewski at al., 2001; Katz et al., 2002; Khaliq et al., 2006; El Adlouni et al., 2007; Ouarda and El Adlouni, 2011). Covariate and time-dependent conditional distributions are then obtained. Such covariates could incorporate whatever drives the variable under study, e.g. trends, cycles or physical variables that can represent atmosphere-ocean patterns (Katz et al., 2002). This approach has gained wide popularity with applications to a large number of hydro-climatic extremes such as rainfall (Thiombiano et al., 2017, 2018; Ouarda et al., 2018), floods (Villarini et al., 2009), wind speeds (Hundecha et al., 2008), air temperatures (Wang et al., 2013, Ouarda and Charron, 2018) and sea wave heights (Wang and Swail, 2006).

The introduction of covariates in the frequency analysis process introduces additional difficulties in the estimation of the parameters of the model. It also introduces an additional stage in the estimation process: Aside from the identification of the appropriate distribution, it is necessary to identify the level of complexity of the dependence relationship between the covariates and the parameters, before proceeding to the estimation process. El Adlouni and Ouarda (2009) proposed a procedure based on the birth-death Markov chain Monte Carlo technique which allows combining the identification of the optimal dependence relationship between covariates and parameters, and the estimation process into a single step.

There is some debate as to whether nonstationary models provide more reliable estimates in practical applications. Milly et. al. (2008) pleaded for an extensive use of nonstationary models instead of the stationary models for water management in the context of climate change. A number of authors (for instance Lins et al., 2011; Serinaldi and Kilsby, 2015), while recognizing that nonstationarity exists, criticized nonstationary models and claimed that stationary models should not be abandoned. Serinaldi and Kilsby (2015) provided a critical overview of the concepts and methods used in nonstationary frequency analysis. They reported that uncertainty can be very large given the increase in complexity of nonstationary models. They stressed out the importance of a fair comparison of the models through the assessment of sampling uncertainties. Ganguli and Coulibaly (2017) investigated nonstationarities and trends in short-duration precipitation extremes in selected urbanized locations in Southern Ontario, Canada, and indicated that the nonstationarity signature in rainfall extremes does not necessarily imply the use of nonstationary IDFs for design purposes. Ganguli and Coulibaly (2019) used RCP8.5 scenario projections for the same study area and found a significant increase in shorter return levels using both stationary and nonstationary frequency analysis methods and a detectable trend was noted for longer return period estimates.

The present work proposes to study the uncertainties associated to stationary and nonstationary models. A comparison of the uncertainties in the estimation of hydro-climatic variables obtained with nonstationary and stationary models is carried out based on observed data. Uncertainties are quantified by the mean of confidence intervals computed by parametric bootstrapping. The case study consists in data from three rainfall stations in the United Arab Emirates (UAE), a region characterised by a desert environment and not often studied.

The rainfall regime of the UAE was studied in Ouarda et al. (2014). The total annual rainfall, the annual maximum rainfall and the number of rainy days per year were analyzed at a number of relatively long-record meteorological stations. While the analysis of trends performed with the Mann-Kendall test indicated slight downward trends for the annual time series, the application of a multiple change point detection procedure revealed that a shift occurred around 1999 with positive trends for the two subsamples before and after the change point. To cope with the presence of the shift, separate frequency analyses with the data samples before and after the change point can be performed, although this reduces the sample sizes considerably. However, the positive trends detected in the subsamples still violate the *iid* assumption.

Evidence of the influence of climate oscillation patterns on precipitation in the region surrounding the UAE has been established in a few studies. A link between precipitation in Iran and the El Niño Southern Oscillation (ENSO) phenomenon were established by Nazemosadat and Ghasemi (2004), and Dezfuli et al. (2010). Also in Iran, Ghasemi and Khalili (2008) analyzed the relationship between several global atmospheric patterns and winter precipitation, and found that the indices with the strongest impacts are the North Sea-Caspian, the Western Mediterranean Oscillation and the North Atlantic Oscillation (NAO) indices. A link between precipitation in the Middle East and NAO was also shown in Cullen et al. (2002). The relationship between rainfall in India and ENSO was established by Krishnamurthy and Goswami (2000), Ashok and Saji (2007), and Dimri (2013), and with Indian Ocean dipole (IOD) by Ashok and Saji (2007).

Recently, a number of studies have focused on the study of the climate of the UAE. Ouarda et al. (2014) demonstrated the strong impact that the ENSO phenomenon has on precipitation over the UAE. They indicated that the observed change in the precipitation regime around 1999 is also caused by ENSO. Niranjan Kumar and Ouarda (2014) concluded that the major portion of the precipitation variability is influenced by equatorial Pacific sea surface temperatures associated with ENSO. In Chandran et al. (2015), the relation of precipitation in the UAE with several global climate oscillations was investigated using wavelet and crosswavelet analysis. The authors found also that global climate oscillations related to ENSO have a strong impact. According to the same study, other climate oscillations that have important impacts are the IOD and the Pacific Decadal Oscillation (PDO). Naizghi and Ouarda (2017) examined the long-term variability of wind speed in the UAE and its teleconnections with various global climate indices. Wavelet coherence analysis demonstrated that wind speed in the UAE is mainly associated with the NAO, East Atlantic (EA) pattern, ENSO and the IOD indices.

In the present study, total annual rainfall and annual maximum rainfall quantiles in the UAE are estimated using stationary and nonstationary approaches. Time and climate indices related to global climate oscillation patterns influencing precipitation in the UAE are introduced as covariates in nonstationary models. An investigation of the relationship between rainfall and a wide selection of climate oscillation indices is conducted to identify the most relevant indices. Cases with a single covariate or a combination of two covariates are considered. The Generalized Extreme Value (GEV) distribution is considered to model annual maxima while the gamma (G) distribution is considered to model annual totals. Models are compared with the Akaike Information Criterion (AIC) (Akaike, 1973).

2. Data

2.1. Study region

The UAE is located in the South-eastern part of the Arabian Peninsula. It is bordered by the Persian Gulf in the north, Oman in the east and Saudi Arabia in the south. The total area of the UAE is about 83600 km^2, 80% of which is desert. The rest is occupied by the mountainous region in the Northeastern part of the country and by the marine coastal regions. The climate of the UAE is arid with very high temperatures in summer. Rainfall is scarce and shows a high temporal and spatial variability. Over 80% of the annual rainfall occurs during the winter period between December and March. The mean annual rainfall in the UAE is about 78 mm ranging from 40 mm in the southern desert region to 160 mm in the northeastern mountains (FAO, 2008). The selected case study allows dealing with a region that is not well studied in the literature, with data series of commonly encountered size and quality, and with a rainfall regime that is characterized by a large variability.

Data from three meteorological stations located in the main international airports of the UAE, where total rainfall is recorded on a daily basis, is used in the present study. Fig. 1 provides the spatial distribution of the meteorological stations. The station of Ras Al Khaimah is located near the north-eastern mountainous region while the Abu Dhabi and Dubai stations are located along the northern coastline. The western region of the country is not represented by any meteorological stations. The three meteorological stations used in the present study were selected based on the length of their records.

A list of the rainfall stations with coordinates, measurement periods and annual rainfall data basis statistics is presented in Table 1. Periods of record range from 30 to 37 years. This represents a situation that is common in hydro-climatology. The last years of data are not available as data needs first to be homogenized. On average, Abu Dhabi receives the smallest amount of rain (63 mm) and Ras Al Khaimah receives the highest amount (127 mm). Minimum total annual rainfall amounts are around zero for all stations. The variability of annual rainfall time series is high for all stations with values of the coefficient of variation reaching nearly one. All skewness values are positive indicating right skewed distributions.

2.2. Rainfall series

From the recorded daily data, the total annual rainfall and the annual maximum daily rainfall were computed for each meteorological station. The use of the calendar year (January 1st to December 31st) to compute annual rainfall series would have resulted in splitting the rainy season between two years. In the present study, the hydrological year starting on September 1st and ending on August 31th has been considered instead for the computation of annual rainfall series.

In Ouarda et al. (2014), a change point analysis was performed on the annual rainfall series with a Bayesian multiple change point procedure (Seidou and Ouarda, 2007). A change point around 1999 was detected for all time series. Fig. 2 illustrates examples of rainfall annual series for the total annual rainfall at Abu Dhabi and for the annual maximum rainfall at Ras Al Khaimah. The general pattern shows that there is a positive trend from the beginning of the series to around 1999, followed by a downward shift and another positive trend until the end. Fig. 3 shows box plots of the samples before and after the change point. In the case of every single time series, we observe an important decrease in the precipitation amount. The shift in the mean, evaluated with the Student's *t*-test, was found to be significant for the total annual rainfall but not for the maximum annual rainfall. The change in the variance was evaluated with the Levine's test and revealed a decrease in the variance for the stations of Abu Dhabi and Dubai for the total annual rainfall.

2.3 Climate indices

Table 2 lists selected climate indices that could potentially be used as covariates in the nonstationary model. A majority of climate indices used in this study was obtained from the Earth System Research Laboratory (ESRL)'s Physical Sciences Division (https://www.esrl.noaa.gov/psd/): the Atlantic Multidecadal Oscillation (AMO), the Arctic Oscillation (AO), the Globally Integrated Angular Momentum (GIAM), the Multivariate ENSO Index (MEI), the North Atlantic Oscillation (NAO), the Oceanic Niño Index (ONI), the Pacific North American Index (PNA), and the Southern Oscillation Index (SOI), the Northern Oscillation Index (NOI), the Pacific Decadal Oscillation (PDO), the Tropical Northern Atlantic Index (TNA), the Tropical Southern Atlantic Index (TSA), and the Western Hemisphere Warm Pool (WHWP). Other climate indices were obtained from the Climate Prediction Center (CPC) at the National Centers for Environmental Prediction (NCEP; https://www.cpc.ncep.noaa.gov/): the East Atlantic Pattern (EA) and the Madden-Julian Oscillation (MJO) pattern. For MJO, the pair of principal component time series, the Real-time Multivariate MJO series 1 and 2 (RMM1 and RMM2), as well as the amplitude of the two MJO principal components (i.e.: $\sqrt{\mathrm{RMM1}^2 + \mathrm{RMM2}^2}$) are used as climate indices.

The Dipole Mode Index (DMI) is used to represent the Indian Ocean Dipole (IOD) phenomenon. Data for DMI was obtained from the Japan Agency for Marine-Earth Science and Technology (http://www.jamstec.go.jp). Data for the Mediterranean Oscillation Index (MOI) was obtained from the Climatic Research Unit at the University of East Anglia (https://crudata.uea.ac.uk). The majority of these indices are available on a monthly basis. RMM1, RMM2 and MOI, being available on a daily basis were averaged over each month to obtain monthly series.

3. Probability distribution assessment

The choice of the distributions to model rainfall variables is justified by the literature and the use of L-moment ratio diagrams. The L-moment ratio diagram is often used to select suitable pdfs to model time series. L-moment ratio diagrams, introduced by Hosking (1990), are commonly used in hydro-climatology (Javelle et al., 2003; Khaliq et al., 2005; Ouarda et al., 2016; Ouarda and Charron, 2019). On the L-moment ratio diagram, the 4th L-moment ratio τ_4 is represented on the *y*-axis and the 3th L-moment ratio τ_3 is represented on the *x*-axis. For each pdf, all possible values of τ_4 versus τ_3 are plotted on the diagram. Distributions with only location and/or scale parameters plot as a single point, distributions with an additional shape parameter plot as a line and distributions with two or more shape parameters cover a whole area in the L-moment ratio diagram. The moment ratios τ_4 and τ_3 are computed for the sample data and are represented by points in the moment ratio diagram. The positions of the samples in the diagram are used to infer on the most suitable pdfs.

In general, it has been observed that the GEV fits best the annual maximum rainfall data (Adamowski, 1996; Endreny and Pashiardis, 2007; Eslamian and Feizi, 2007; Lee and Maeng, 2003; Abolverdi and Khalili, 2010; Cheng & AghaKouchak, 2014). For the total annual rainfalls, the G, GEV, Log-Pearson 3 (LP3) and Pearson 3 (P3) are the most frequently used distributions (Örztürk, 1981; Ben-Gai et al., 2001; Small et al., 2007; Yue and Hashino, 2007; Gonzalez and Valdés, 2008; Hallack-Ageria et al., 2012). Fig. 4 presents the L-moment ratio diagrams with the sample moments for each station for the annual maxima and the annual totals. Candidate distributions considered are the Weibull (W), G or P3, Lognormal (LN), Generalized Pareto (GPA) and GEV. For the annual maximum rainfall time series, the GEV is found to be the most suitable pdf, as the samples of the three stations are located near the curve of the GEV. For the total rainfall time series, the G is found to be the most suitable distribution as the samples of the Ras Al Khaimah and Dubai stations are located directly on the curve of the G distribution, while for the sample of the Abu Dhabi station, the G is among the pdfs leading to the best fit.

4. Methods

4.1. Nonstationary models

The cumulative distribution function (cdf) of the GEV is defined by (Coles, 2001):

$$F_{GEV}(x;\mu,\sigma,\kappa)=\begin{cases}\exp\left[-\left(1+\dfrac{\kappa}{\sigma}(x-\mu)\right)^{-1/\kappa}\right], & \kappa\neq 0\\ \exp\left[-\exp\left(-\dfrac{(x-\mu)}{\sigma}\right)\right], & \kappa=0\end{cases} \tag{1}$$

where μ, σ and κ are location, scale and shape parameters respectively, and $\mu-\sigma/\kappa\leq x<\infty$ for $\kappa>0$, $-\infty<x<+\infty$ for $\kappa=0$ and $-\infty<x\leq\mu-\sigma/\kappa$ for $\kappa<0$. In the nonstationary case, the distribution parameters are expressed as a function of time dependent covariates: $\mu=\mu_t$ and $\sigma=\sigma_t$. Given the time dependent covariate Y_t (which can represent a climate oscillation index), the following nonstationary models are defined in this study:

GEV10 $\quad \mu_t=a_0+a_1Y_t$ and $\sigma_t=\sigma$, (2a)

GEV01 $\quad \mu_t=\mu$ and $\ln(\sigma_t)=b_0+b_1Y_t$, (2b)

GEV11 $\mu_t = a_0 + a_1 Y_t$ and $\ln(\sigma_t) = b_0 + b_1 Y_t$, (2c)

GEV20 $\mu_t = a_0 + a_1 Y_t + a_2 Y_t^2$ and $\sigma_t = \sigma$, (2d)

GEV21 $\mu_t = a_0 + a_1 Y_t + a_2 Y_t^2$ and $\ln(\sigma_t) = b_0 + b_1 Y_t$. (2e)

where *a* and *b* are coefficients to estimate. The shape parameter is kept constant ($\kappa_t = \kappa$) as trends in the location and scale parameters are generally more important and κ is also very difficult to estimate in the presence of small sample sizes (Khaliq et al., 2006). The first index in the model notation in Eqs. 2 refers to the order of the location parameter and the second index refers to the order of the scale parameter. The stationary case model is denoted GEV00 where the location parameter μ_t and the scale parameter σ_t are constant ($\mu_t = \mu$, $\sigma_t = \sigma$). The scale parameter, for models introducing a covariate, is logarithmically transformed to ensure positive values.

The cdf of the G is defined by:

$$F_G(x; a, b) = \frac{1}{\beta^\alpha \Gamma(\alpha)} \int_0^x t^{\alpha-1} e^{-t/\beta} dt \tag{3}$$

where β and α are the scale and shape parameters respectively, and $\beta > 0$ and $\alpha > 0$. In the nonstationary case, the scale parameter is expressed as a function of time dependent covariates: $\beta = \beta_t$. Given the time dependent covariate Y_t (which can represent a climate oscillation index), the following nonstationary models are defined in this study:

G1 $\ln(\beta_t) = a_0 + a_1 Y_t$, (4a)

G2 $\ln(\beta_t) = a_0 + a_1 Y_t + a_2 Y_t^2$ (4b) where a are coefficients to estimate. The shape parameter is also kept constant ($\alpha_t = \alpha$) for the same reasons as for the GEV. The stationary case model is denoted G0 where the scale parameter is constant ($\beta_t = \beta$). The scale parameter is logarithmically transformed to ensure positive values.

The nonstationary case with two covariates is also considered. Given an additional covariate Z_t, the distribution parameters depend then on the two covariates Y_t and Z_t. Different combinations of these covariates for the distribution parameters are considered. In the present study, we consider a linear and quadratic relation for the location parameter, and a linear relation for the scale parameter. The nonstationary GEV models with two covariates are denoted GEV(i_Y-i_Z, j_Y-j_Z) where i_Y-i_Z represents the dependency of the location parameter on the covariates Y_t and Z_t, and j_Y-j_Z represents the dependency of the scale parameter on the covariates. For instance, the model GEV(2-1,1-1) indicates that the location parameter has a quadratic relation with the first covariate and a linear relation with the second covariate, and that the scale parameter has a linear relation with both the first and the second covariate (i.e., $\mu_t = a_0 + a_1 Y_t + a_2 Y_t^2 + a_3 Z_t$, $\ln(\sigma_t) = b_0 + b_1 Y_t + b_2 Z_t$). The nonstationary G models with two covariates are denoted G(i_Y-i_Z) where i_Y-i_Z represents the dependency of the scale parameter on the covariates.

4.2. Parameter estimation

The parameter vectors θ of these models are estimated with the maximum likelihood method (ML). For a given pdf denoted f, the likelihood function for the sample $x = \{x_1, ..., x_n\}$ is:

$$L_n = \prod_{t=1}^{n} f(x_t; \theta). \quad (5)$$

The optimization function *fminsearch* in MATLAB (MATLAB, 2014) is used to obtain $\hat{\theta}$, the estimator of θ, that maximizes the likelihood function L_n. To compare the goodness-of-fit of the different models, the Akaike information criterion (AIC) is used. It is defined by:

$$\mathrm{AIC} = -2\ln(L_n) + 2k \tag{6}$$

where k is the number of parameters of the model. This statistic accounts for the goodness-of-fit of the model and also for the parsimony through the parameter k whose value increases with the model complexity.

4.3. Confidence intervals

The confidence interval (CI) of an estimated value tells how accurate the estimation is. A commonly used method to compute CIs is the bootstrap. It is a data-based simulation method that allows to make statistical inference on CIs. The method adopted in this study for the computation of the CIs of the estimated quantiles is the parametric bootstrap as described in Efron and Tibshirani (1993). In this method, a parametric estimate $\hat{F}$ of the population F with a sample size of n is first obtained. Subsequently, B samples of size n are drawn from the parametric estimate $\hat{F}$. Then, for each sample, model parameters $\hat{\theta}_b$, $b = 1, 2, ..., B$, are estimated and quantiles $\hat{q}_b = F^{-1}(p; \hat{\theta}_b)$ are evaluated. Finally, the CI around $\hat{q}$ is computed using the standard deviation of the B estimated quantiles $\hat{q}_b$.

5. Results and discussion

Prior to carrying out the nonstationary frequency analysis, two covariates representing climate indices are selected to be included in the nonstationary models. A climate index covariate is defined by the average of an index over a season of 3 consecutive months. A season is denoted here by the three first letters of the 3 months included. Seasonal climate index series were built by averaging moving consecutive 3-months windows for the candidate climate indices in Table 2. The correlations between the different seasonal climate index series and the annual rainfall series were investigated in order to select the most relevant covariates. Table 3 presents the Pearson correlation coefficients for the total annual rainfall series in Abu Dhabi from the season of April-May-June (AMJ*) of the previous hydrological year until March-April-May (MAM) of the same hydrological year than the rainfall events. In Table 3 and in the remainder of the paper, * denotes a season before the hydrological year (September 1st to August 31st) corresponding to the rainfall events. Significant correlations at the 5% level are denoted in bold characters in Table 3. Similar results were obtained for the maximum rainfall and thus are not presented here

Covariates are selected based on the significance of the correlations between the rainfall series and the seasonal climate indices. As the interest here is the prediction of rainfalls, covariates were selected during a season preceding the period of December to Mars, which corresponds to the rainy season in the UAE. The climate indices having one or more seasons with a significant correlation with rainfalls are GIAM, MEI, NOI, ONI, PDO, SOI, DMI and MOI. The choice of a covariate within these climate indices was validated with the scatter plots of the rainfall variables versus the covariate. This validation is required after an initial selection as the significance test does not guaranty a causal relationship: The probability of concluding to a significant correlation while it is in fact false is equal to the chosen significance level of 5%. This validation allowed to discard the indices PDO, DMI and MOI. Indeed, even though correlations are high for some seasons, the scatter plots for these indices revealed incoherent patterns. For instance, for the PDO index, the correlations are positive but for some cases, the rainfall values are very low even though the corresponding values of this climate index are very high. Retained indices after this validation were GIAM, MEI, NOI, ONI and SOI. All these indices are related to ENSO, proving that this phenomenon is the main oscillation pattern explaining the variance of the precipitation in the region.

ONI and NOI for the season JJA*, denoted by ONI(JJA*) and NOI(JJA*), were the selected covariates. ONI(JJA*) was selected because it has one of the highest correlations with the rainfall series. For the selection of the second covariate, intercorrelations between climate indices were checked to avoid the selection of indices that are too similar and reduce redundancy. NOI(JJA*) was selected second because, of all the climate indices retained, NOI has the smallest correlation with ONI (-0.51). Fig. 5 presents the correlations between the total annual rainfall at the three rainfall stations and the three-month moving averages of ONI and NOI. It shows that correlations increase as the index window becomes closer to the rainfall season. Correlations remain significant for several seasons. Finally, correlations decrease to become insignificant towards the end of the rainfall season. The correlations for Dubai are significantly lower than for the other stations. Scatter plots of selected covariates with the total annual rainfall at Abu Dhabi and the maximum annual rainfall at Ras Al Khaimah are presented in Fig. 6 as examples. These graphs confirm the choice of the covariates by showing that the rainfall series have coherent relationships with the covariates.

The stationary model, the nonstationary model including time as a covariate, and the nonstationary models including each or both selected climate index covariates were fitted to the annual rainfall series. For comparison purposes, the GEV model was also applied to total rainfalls.

Table 4 presents the values of the AIC criterion obtained for each model. For the nonstationary cases, only the result corresponding to the model leading to the best fit according to AIC is presented. Overall, results indicate that the G model is more appropriate than the GEV for total rainfalls except for Dubai where AIC are lower for the GEV than the G. Results show that adding the time as a covariate reduces in general the goodness-of-fit in comparison to the stationary model. When including a climate index covariate, a better fit than the stationary model is generally obtained. When including ONI and NOI together, the overall best fit is often obtained. The models with time and a climate index as covariates do not generally improve the goodness-of-fit compared to the model with the climate index only.

Figs. 7-8 present the quantiles corresponding to the non-exceedance probabilities of p = 0.25, 0.5 and 0.75 as a function of the covariate for selected nonstationary models with one covariate. The representation of three quantiles allows to observe changes in both the trend and the variance. Observed data points are also presented in these figures. In each case, the model leading to the best fit is illustrated (see Table 4). The quantiles obtained with the stationary model are also presented in each figure for comparison purposes.

Fig. 7a illustrates the quantiles for the total annual rainfall in Abu Dhabi as a function of the time for the nonstationary G model using time as a covariate and fitted to the data over the whole period. The model G1 is retained as the best model. In this case, the variance of the distribution decreases with time due to the negative trend in the scale parameter. It can be observed that quantile values are very small during the last years. They represent bad values for design or management purposes. The nonstationary model with time was also fitted separately to the samples before and after the change point in 1999. The model G1 was retained as the best model for both samples. An example for the total annual rainfall in Abu Dhabi is presented at Fig. 7b. Quantile values during the last year are also very low as only the portion of the data with reduced rainfall was used.

Fig. 8a presents the quantiles for the total annual rainfall in Abu Dhabi as a function of the covariate ONI(JJA*) and Fig. 8b presents the quantiles for the annual maximum rainfall in Ras Al Khaimah as a function of the covariate NOI(JJA*). The models G1 and GEV20 are respectively retained as the best models. The variance of quantile values shows accordingly a constant increase with ONI in Fig. 8a. A large variation in quantile values as a function of the covariate can be observed in both figures: Quantile values of the median total rainfalls range from about 20 mm to 100 mm, and quantile values of the median maximum rainfalls range from about 20 mm to 75 mm. There is a change in the sign of slopes of the quantile curves at the minimum rainfall in the case of maximum rainfalls. This cannot obviously be explained by a climatic phenomenon. This is rather caused by the lack of data for events corresponding to extreme values of the climate indices.

The surface plot of the quantiles corresponding to nonexceedance probabilities of $p = 0.5$ and 0.75 for the total and maximum annual rainfall in Abu Dhabi and Ras Al Khaimah as a function of both climate index covariates are presented as examples in Fig. 9. Even though the fit is increased with the two covariates, some problems can be noticed in the graphs of Fig. 9. It was shown in Figs. 6 and 8 that rainfalls generally increase with ONI and decrease with NOI. While these relations are respected for total rainfalls, they are not always respected for maximum rainfalls in Fig. 9. Indeed, maximum rainfall quantiles for $p = 0.5$ and 0.75 increase with NOI in Abu Dhabi (Fig. 9c), and maximum rainfall quantiles for $p = 0.75$ decrease with ONI in Ras Al Khaimah (Fig. 9d). These problems may indicate that the number of model parameters is too high in the case of the nonstationary GEV model for the size of the data sample and that causes overfitting of the data. This may indicate here that the limits of some models are reached.

The use of one or the other models presented previously has a strong impact on the estimated rainfall quantiles at a given time. A comparison of the quantile estimates that would be obtained for 2012, the year following the last observed record data, using different models is conducted at the station of Abu Dhabi. Fig. 10 presents, with bar graphs, the predicted quantiles for the probabilities p = [0.5, 0.8, 0.9, 0.95, 0.98, 0.99] corresponding to the classical return periods of 2, 5, 10, 20, 50 and 100 years. Quantiles are defined for nonexceeding probabilities here because under the nonstationary framework, the classical definition of return period is not appropriate (El Adlouni et al., 2007; Salas and Obeysekera, 2014). The following scenarios are considered: the stationary case, the nonstationary case with time as covariate, the nonstationary case with the covariate ONI(JJA*) and the nonstationary case with the two climate index covariates. For total rainfalls, only the G model results are presented. For the stationary model and the nonstationary model with time, the models are fitted to the sample defined by the whole observed period, as well as to the subsample from 1983 to 1998 and to the subsample from 1999 to 2011. These subsamples correspond to the data before and after the change point of 1999. For all the nonstationary models, the quantiles presented in Fig. 10 are those predicted for the year 2012. For the nonstationary case with time, the quantiles based on the model fitted for the period 1983-1998 correspond hence to an extrapolation from 1998 to 2012, and those based on the model fitted for the period 1983-2011, to an extrapolation from 2011 to 2012. For the nonstationary models with climate indices, the values of the covariates ONI(JJA*) and NOI(JJA*) are respectively -0.19 and -0.10.

It can be observed in Fig. 10 that there are large differences in the predicted quantiles for the different scenarios. Using only the sample from 1999-2011 results in an underestimation of the quantiles compare to those obtained using the sample for the entire period in either the stationary case or the nonstationary case with time as covariate. This is caused by the fact that observed rainfalls were weaker during the last years (See Fig. 7). Using only the sample from 1983-1998 with the nonstationary model using time as a covariate results in an overestimation of the quantiles compare to those obtained using the sample for the entire period. This is caused by the extrapolation occurring from 1998 to 2012. As the best fits were obtained with nonstationary models including climate indices, the most realistic scenarios should hence be represented by the models including climate indices as covariates. The values of the climate indices used as covariates for 2012 predict a year of low precipitation. As a result, quantiles obtained with the model with one climate index are lower than those corresponding to the stationary model fitted over the whole period. In fact, the nonstationary model with one climate index predicts quantiles that are among the lowest of all scenarios for both rainfall variables. With two climate indices, the quantiles for total rainfalls compare to those obtained with the model with one climate index. For maximum rainfalls, the quantiles compare to those with the model with one climate index for the lowest probabilities but as the probability increases, the quantiles for the model with two covariates become much higher. For maximum rainfall, quantiles become even larger than the stationary case for $p \geq 0.95$. This is suspicious as climate indices indicate a year with lower precipitation than usual. This last result indicates potential problems with the GEV model with two covariates when quantiles are extrapolated to extreme probabilities. These problems were already noticed in Fig. 9. The remainder of this section will look at the cause of these behaviors.

Previous results showed that the nonstationary models with climate indices provide better fits to the data. However, this is true only for frequencies within the range of those observed during the period of record. In frequency analysis, to estimate quantiles corresponding to more extreme probabilities than those observed, we need to extrapolate in the frequency domain. With nonstationary models, additional extrapolation may occur in the domains of the covariates.

Nonstationary models introduce also supplementary sources of uncertainties: They require the estimation of a larger number of parameters and the covariates have measurement errors. For short time series, the impacts of these sources of uncertainties on the reliability of the predicted quantiles can be significant. The remainder of this section will focus on the comparison of quantile uncertainty for stationary models and nonstationary models with one or two climate index covariates. Quantile uncertainty is assessed in this study through CIs computed with the parametric bootstrap method presented in section 4.3.

Fig. 11 presents graphs of the predicted quantiles with the CIs as a function of the nonexceedence probability. The cases of the total rainfalls for the nonstationary models G1 and GEV21 and the maximum rainfalls for the nonstationary model GEV20 in Ras Al Khaimah are illustrated with the covariate NOI(JJA*) taking the values of -2.25 and 0.5. The selected values of the covariate correspond to scenarios of low and high rainfalls (see Fig. 8). In all cases, the width of the CIs increases rapidly with the probability. When $\mathrm{NOI(JJA^*)} = -2.25$, the upper CIs curve for the total rainfalls leads to improbable high rainfall estimations as the probability increases. The G1, a simpler model than GEV21, has an upper CIs curve that is much lower than the one for GEV21. For instance, the width of the CI is accentuated by the negative trend on the scale parameter for model GEV21 which results in a larger variance for extreme negative values of NOI(JJA*). For maximum rainfalls and $\mathrm{NOI(JJA^*)} = -2.25$, the width of the CI for the nonstationary model is larger than the width of the CI for the stationary model at the lowest probabilities (approximatively for $p < 0.95$). For NOI(JJA*) = 0.5 and for both rainfall variables, the widths of the CIs for the nonstationary and the stationary models are comparable. In the cases presented, for the lowest probabilities, the nonstationary model leads to quantiles that are significantly different from the stationary model. As the probability increases, the CIs corresponding to both models overlap in large parts and each CI eventually includes the predicted quantiles of the other.

Fig. 12 presents the quantiles for $p = 0.5$ as a function of NOI(JJA*) for total and maximum annual rainfalls in Ras Al Khaimah using the models G1 and GEV20 respectively. For some ranges of values of the climate index, the CIs overlap in large part and the CIs of the nonstationary model can encompass completely the CIs of the stationary model. For maximum rainfalls and $\mathrm{NOI(JJA^*)} \leq -1.5$, the CIs of both models are totally distinct. The widths of the CIs for the nonstationary model increase as the climate index value becomes more extreme. This is explained by the lack of observed data in the extremes range.

Fig. 13 presents similar graphs to Fig. 11 but for the nonstationary model with two covariates. Two cases with real observed covariate values are illustrated: the year 1988, corresponding to high rainfalls ($\mathrm{ONI(JJA^*)} = 1.41$ and $\mathrm{NOI(JJA^*)} = -2.14$) and the year 2001, corresponding to low rainfalls ($\mathrm{ONI(JJA^*)} = \text{-}0.58$ and $\mathrm{NOI(JJA^*)} = 0.19$). With two covariates, the widths of the CIs for the nonstationary GEV models are much larger than with one covariate. In most cases, this leads to improbable values for the upper CIs in the highest probabilities (approximatively for $p \geq 0.95$). Also, for the highest probabilities, the CIs of nonstationary models overlap in a large part or encompass entirely the CIs of stationary models. For the nonstationary G models, the CIs are similar to those obtained with one covariate. This shows that G is more appropriate than GEV for total rainfalls at Ras Al Khaimah: In addition of giving a better fit, G has narrower CIs with two covariates.

The previous results show that even if the fit is often better with nonstationary models, the uncertainties on quantile estimates associated to these models can be very important. These uncertainties are more important in the extremes range in both the frequency domain and the covariates domains. Because of the importance of these uncertainties, there may be no advantage in using a nonstationary model for certain frequencies or covariate values. When the CIs of the quantiles estimated by the nonstationary model and by the stationary model overlap significantly, the results given by the nonstationary models are judged not sufficiently distinct from those of the stationary model to justify the use of a more complex model. Uncertainties increase significantly with the use of two covariates in the nonstationary model. This is caused by the increased model complexity that often results from the inclusion of an additional covariate and from the measurement errors associated to that covariate. The results of the study demonstrate that nonstationary models should be used with caution. The complexity of nonstationary models should be limited especially with small sample sizes. Extrapolation within the frequency domain should also be limited.

6. Conclusions

Severe nonstationarities were observed in rainfall time series in the UAE: a change in the rainfall regime in 1999 and the presence of trends. This situation represents a challenge for stationary frequency analysis models. To deals with these issues, nonstationary models introducing covariates in the distribution parameters were used.

The nonstationary model including time as a covariate was found to be inefficient given the presence of a change point. Fitting this model separately on the subsamples before and after the change point represent a better solution, but the inconvenient is that the sample size is reduced drastically. Also, a major drawback of using nonstationary models with time as covariate is the increased uncertainty with extrapolation as future trends are not known. On the other hand, nonstationary models including a climate index are more promising. In either case, it is important to have a clear understanding of the dynamics and the phenomena involved. These results agree with Agilan and Umamahesh (2017) where the authors have shown that time may not be the best covariate and that it is important to analyze all possible covariates to model nonstationarity.

The influence of climate oscillation patterns on the hydro-climatological variables over the region has been well established in many studies (Basha et al., 2015; Niranjan Kumar et al., 2016; Kumar et al., 2017). Seasonal climate index series built from moving windows of average consecutive 3-months were correlated with the annual rainfall series. Oscillation patterns related to ENSO were identified as having a major influence over the region. Based on the correlations of the seasonal climate index series with the annual rainfall series, average ONI and NOI during the months of Jun-Jul-Aug were selected as covariates. The selected covariates were introduced separately and together in the nonstationary models. Significant improvements were obtained with a model including at least one climate index compared to the stationary model, and a model including two climate indices gave in general the overall best fit.

The fact that the fit is increased does not guaranty that the predictions are more reliable. With nonstationary models, the complexity is increased because of the additional parameters. The use of two covariates involves even more complex models and the second covariate brings additional measurement errors to the model. To assess the uncertainties, CIs for the predicted quantiles were computed with the parametric bootstrap method. A comparison of the CIs corresponding to the stationary and nonstationary models was conducted.

As the probability increases, the CIs of nonstationary models become wider rapidly and can lead to improbable quantile predictions. With two covariates, uncertainties associated to predicted quantiles can become considerably large. For moderate probabilities, the CIs of predicted quantiles corresponding to stationary and nonstationary models are often distinct, but for high nonexceedance probabilities, the CIs overlap in large parts. For some ranges of values of the climate index used as covariate, the CIs of both models also overlap considerably, even for low probabilities (for instance 0.5). In these cases, the use of the more complex nonstationary model may not be justified as the predictions of both models are similar. Similar conclusions were also obtained in Ganguli and Coulibaly (2017), where despite the presence of nonstationary signals in short-duration rainfall extremes, statistically indistinguishable differences were obtained between stationary and nonstationary return level estimates.

Nonstationary models can still be very useful as they allow to adapt hydro-climatic quantiles to changing conditions. However, they should be used with caution especially with small sample sizes. Indeed, in this case, uncertainties can be very high when quantiles are extrapolated with respect to the return period or the covariate values.

Acknowledgment

The authors thank the National Sciences and Engineering Research Council of Canada (NSERC) and the Canada Research Chair Program for funding this research. The authors wish to thank the UAE National Centre of Meteorology (NCM) for having supplied the data used in this study. The authors are grateful to the Editor, Dr. Radan Huth, to the Associate Editor, Dr. Enric Aguilar, and to two anonymous reviewers for their comments which helped improve the quality of the manuscript.

References

Abolverdi, J., Khalili, D., 2010. Development of Regional Rainfall Annual Maxima for Southwestern Iran by L-Moments. Water Resources Management 24(11), 2501-2526.

Adamowski, K., Alila, Y., Pilon, P.J., 1996. Regional rainfall distribution for Canada. Atmospheric Research 42(1-4), 75-88.

Agilan, V., Umamahesh, N.V., 2017. What are the best covariates for developing non-stationary rainfall Intensity-Duration-Frequency relationship? Advances in Water Resources, 101: 11-22.

Akaike, H., 1973. Information theory and an extension of the maximum likelihood principle. In: Petrov, B.N., Csáki, F. (Ed.), Second International Symposium on Information Theory. Akademinai Kiado, Budapest, Hungary, pp. 267-281.

Ashok, K., Saji, N.H., 2007. On the impacts of ENSO and Indian Ocean dipole events on sub-regional Indian summer monsoon rainfall. Natural Hazards 42(2), 273-285.

Basha, G., Marpu, P.R., Ouarda, T.B.M.J., 2015. Tropospheric temperature climatology and trends observed over the Middle East. Journal of Atmospheric and Solar-Terrestrial Physics, 133: 79-86.

Ben-Gai, T., Bitan, A., Manes, A., Alpert, P., Rubin, S., 1998. Spatial and Temporal Changes in Rainfall Frequency Distribution Patterns in Israel. Theoretical and Applied Climatology, 61(3): 177-190.

Chandran, A., Basha, G., Ouarda, T.B.M.J., 2015. Influence of Climate Oscillations on Temperature and Precipitation over the United Arab Emirates. International Journal of Climatology, 36(1), 225-235.

Cheng, L., AghaKouchak, A., 2014. Nonstationary Precipitation Intensity-Duration-Frequency Curves for Infrastructure Design in a Changing Climate. Scientific Reports, 4: 7093.

Coles, S., 2001. An introduction to statistical modeling of extreme values. Springer, London, 208 pp.

Cullen, H., Kaplan, A., Arkin, P., deMenocal, P., 2002. Impact of the North Atlantic Oscillation on Middle Eastern Climate and Streamflow. Climatic Change 55(3), 315-338.

Dezfuli, A., Karamouz, M., Araghinejad, S., 2010. On the relationship of regional meteorological drought with SOI and NAO over southwest Iran. Theoretical and Applied Climatology 100(1-2), 57-66.

Dimri, A.P., 2013. Relationship between ENSO phases with Northwest India winter precipitation. International Journal of Climatology 33(8), 1917-1923.

Efron, B., Tibshirani, R.J., 1993. An Introduction to the Bootstrap. Chapman & Hall/CRC, New York, 456 pp.

El Adlouni, S., Ouarda, T.B.J.M., Zhang, X., Roy, R., Bobee, B., 2007. Generalized maximum likelihood estimators for the nonstationary generalized extreme value model. Water Resources Research 43(3), W03410.

El Adlouni, S., Ouarda, T.B.M.J., 2009. Joint Bayesian model selection and parameter estimation of the generalized extreme value model with covariates using birth-death Markov chain Monte Carlo. Water Resources Research 45(6), W06403.

Endreny, T.A., Pashiardis, S., 2007. The error and bias of supplementing a short, arid climate, rainfall record with regional vs. global frequency analysis. Journal of Hydrology 334(1-2), 174-182.

Eslamian, S.S., Feizi, H., 2007. Maximum Monthly Rainfall Analysis Using L-Moments for an Arid Region in Isfahan Province, Iran. Journal of Applied Meteorology and Climatology 46(4), 494-503.

FAO, 2008. Irrigation in the Middle East region in figures: AQUASTAT Survey - 2008. water report, 34 pp.

Ganguli, P., Coulibaly, P., 2017. Does nonstationarity in rainfall require nonstationary intensity–duration–frequency curves? Hydrology and Earth System Sciences, 21(12): 6461-6483.

Ganguli, P., Coulibaly, P., 2019. Assessment of future changes in intensity-duration-frequency curves for Southern Ontario using North American (NA)-CORDEX models with nonstationary methods. Journal of Hydrology: Regional Studies, 22: 100587.

Ghasemi, A.R., Khalili, D., 2008. The association between regional and global atmospheric patterns and winter precipitation in Iran. Atmospheric Research 88(2), 116-133.

Gonzalez, J., Valdes, J.B., 2008. A regional monthly precipitation simulation model based on an L-moment smoothed statistical regionalization approach. Journal of Hydrology, 348(1-2): 27-39.

Hallack-Alegria, M., Ramirez-Hernandez, J., Watkins, D.W., 2012. ENSO-conditioned rainfall drought frequency analysis in northwest Baja California, Mexico. International Journal of Climatology 32(6), 831-842.

Hosking, J.R.M., 1990. L-Moments: Analysis and estimation of distributions using linear combinations of order statistics. Journal of the Royal Statistical Society. Series B (Methodological) 52(1), 105-124.

Hundecha, Y., St-Hilaire, A., Ouarda, T.B.M.J., El Adlouni, S., Gachon, P., 2008. A Nonstationary Extreme Value Analysis for the Assessment of Changes in Extreme Annual Wind Speed over the Gulf of St. Lawrence, Canada. Journal of Applied Meteorology and Climatology 47(11), 2745-2759.

Javelle, P., Ouarda, T.B.M.J., Bobée, B., 2003. Spring flood analysis using the flood-duration–frequency approach: application to the provinces of Quebec and Ontario, Canada. Hydrological Processes, 17(18): 3717-3736.

Katz, R.W., Parlange, M.B., Naveau, P., 2002. Statistics of extremes in hydrology. Advances in Water Resources 25(8–12), 1287-1304.

Khaliq, M.N., Ouarda, T.B.M.J., Ondo, J.C., Gachon, P., Bobée, B., 2006. Frequency analysis of a sequence of dependent and/or non-stationary hydro-meteorological observations: A review. Journal of Hydrology 329(3–4), 534-552.

Khaliq, M.N., St-Hilaire, A., Ouarda, T.B.M.J., Bobée, B., 2005. Frequency analysis and temporal pattern of occurrences of southern Quebec heatwaves. International Journal of Climatology, 25(4): 485-504.

Krishnamurthy, V., Goswami, B.N., 2000. Indian monsoon-ENSO relationship on interdecadal timescale. Journal of Climate 13(3), 579-595.

Kumar, K.N., Molini, A., Ouarda, T.B.M.J., Rajeevan, M.N., 2017. North Atlantic controls on wintertime warm extremes and aridification trends in the Middle East. Scientific Reports, 7(1): 12301.

Lee, S.H., Maeng, S.J., 2003. Frequency analysis of extreme rainfall using L-moment. Irrigation and Drainage 52(3), 219-230.

Lins, H.F., Cohn, T.A., 2011. Stationarity: Wanted Dead or Alive? JAWRA Journal of the American Water Resources Association 47(3), 475-480.

MATLAB, 2014. version 8.3.0 (R2014a). The MathWorks Inc., Natick, Massachusetts.

Milly, P.C.D., Betancourt, J., Falkenmark, M., Hirsch, R.M., Kundzewicz, Z.W., Lettenmaier, D.P., Stouffer, R.J., 2008. Stationarity Is Dead: Whither Water Management? Science 319(5863), 573-574.

Naizghi, M.S., Ouarda, T.B.M.J., 2017. Teleconnections and analysis of long-term wind speed variability in the UAE. International Journal of Climatology, 37(1): 230-248.

Nazemosadat, M.J., Ghasemi, A.R., 2004. Quantifying the ENSO-Related Shifts in the Intensity and Probability of Drought and Wet Periods in Iran. Journal of Climate 17(20), 4005-4018.

Niranjan Kumar, K., Ouarda, T., 2014. Precipitation variability over UAE and global SST teleconnections. Journal of Geophysical Research: Atmospheres 119(17), 10,313-10,322.

Niranjan Kumar, K., Ouarda, T.B.M.J., Sandeep, S., Ajayamohan, R.S., 2016. Wintertime precipitation variability over the Arabian Peninsula and its relationship with ENSO in the CAM4 simulations. Climate Dynamics, 47(7-8): 2443-2454.

Öztürk, A., 1981. On the Study of a Probability Distribution for Precipitation Totals. Journal of Applied Meteorology, 20(12): 1499-1505.

Ouarda, T.B.M.J., Charron, C., 2018. Nonstationary Temperature-Duration-Frequency curves. Scientific Reports, 8(1): 15493.

Ouarda, T.B.M.J., Charron, C., 2019. Changes in the distribution of hydro-climatic extremes in a non-stationary framework. Scientific Reports, 9(1): 8104.

Ouarda, T.B.M.J., Charron, C., Chebana, F., 2016. Review of criteria for the selection of probability distributions for wind speed data and introduction of the moment and L-moment ratio diagram methods, with a case study. Energy Conversion and Management, 124: 247-265.

Ouarda, T.B.M.J., Charron, C., Niranjan Kumar, K., Marpu, P.R., Ghedira, H., Molini, A., Khayal, I., 2014. Evolution of the rainfall regime in the United Arab Emirates. Journal of Hydrology 514(0), 258-270.

Ouarda, T.B.M.J., El-Adlouni, S., 2011. Bayesian Nonstationary Frequency Analysis of Hydrological Variables. JAWRA Journal of the American Water Resources Association 47(3), 496-505.

Ouarda, T.B.M.J., Yousef, L.A., Charron, C., 2019. Non-stationary intensity-duration-frequency curves integrating information concerning teleconnections and climate change. International Journal of Climatology 39(4), 2306-2323.

Salas, J., Obeysekera, J., 2014. Revisiting the Concepts of Return Period and Risk for Nonstationary Hydrologic Extreme Events. Journal of Hydrologic Engineering 19(3), 554-568.

Seidou, O., Ouarda, T.B.M.J., 2007. Recursion-based multiple changepoint detection in multiple linear regression and application to river streamflows. Water Resources Research 43(7), W07404.

Serinaldi, F., Kilsby, C.G., 2015. Stationarity is undead: uncertainty dominates the distribution of extremes. Advances in Water Resources 77, 17-36.

Small, D., Islam, S., 2007. Decadal variability in the frequency of fall precipitation over the United States. Geophysical Research Letters, 34(2), L02404.

Strupczewski, W.G., Singh, V.P., Feluch, W., 2001. Non-stationary approach to at-site flood frequency modelling I. Maximum likelihood estimation. Journal of Hydrology 248(1–4), 123-142.

Thiombiano, A.N., El Adlouni, S., St-Hilaire, A., Ouarda, T.B.M.J., El-Jabi, N., 2017. Nonstationary frequency analysis of extreme daily precipitation amounts in Southeastern Canada using a peaks-over-threshold approach. Theoretical and Applied Climatology, 129(1-2): 413-426.

Thiombiano, A.N., St-Hilaire, A., El Adlouni, S.-E., Ouarda, T.B.M.J., 2018. Nonlinear response of precipitation to climate indices using a non-stationary Poisson-generalized Pareto model: case study of southeastern Canada. International Journal of Climatology, 38(S1): e875-e888.

Villarini, G., Smith, J.A., Serinaldi, F., Bales, J., Bates, P.D., Krajewski, W.F., 2009. Flood frequency analysis for nonstationary annual peak records in an urban drainage basin. Advances in Water Resources 32(8), 1255-1266.

Wang, X.L., Swail, V.R., 2006. Climate change signal and uncertainty in projections of ocean wave heights. Climate Dynamics 26(2-3), 109-126.

Wang, X.L., Trewin, B., Feng, Y., Jones, D., 2013. Historical changes in Australian temperature extremes as inferred from extreme value distribution analysis. Geophysical Research Letters 40(3), 573-578.

Yue, S., Hashino, M., 2007. Probability distribution of annual, seasonal and monthly precipitation in Japan. Hydrological Sciences Journal 52(5), 863-877.

Tables

Table 1. Description of rainfall stations and characteristics of total annual rainfall time series. Minimum, maximum, mean, dimensionless L-moment ratios of variation (τ_2), skewness (τ_3) and kurtosis (τ_4).

Station name	Latitude	Longitude	Altitude (m)	Period	Years	Min (mm)	Max (mm)	Mean (mm)	τ_2	τ_3	τ_4
Abu Dhabi Int'l Airport	24°26' N	54°39' E	27	1982-2011	30	0.0	226	63	0.50	0.26	0.09
Dubai Int'l Airport	25°15' N	55°20' E	8	1975-2011	37	0.3	355	93	0.44	0.26	0.14
Ras Al Khaimah Int'l Airport	25°37' N	55°56' E	31	1976-2011	36	0.0	461	127	0.42	0.22	0.14

Table 2. Potential climate indices to be used as covariates in nonstationary models.

Climate index name	Symbol
Atlantic Multidecadal Oscillation	AMO
Arctic Oscillation	AO
Dipole Mode Index (Indian Ocean Dipole)	DMI
East Atlantic Pattern	EA
Globally Integrated Angular Momentum	GIAM
Multivariate ENSO Index	MEI
Madden-Julian Oscillation (Amplitude)	MJO(amp)
Mediterranean Oscillation Index	MOI
North Atlantic Oscillation	NAO
Northern Oscillation Index	NOI
Oceanic Niño Index	ONI
Pacific Decadal Oscillation	PDO
Pacific North American Index	PNA
Real-time Multivariate MJO series1	RMM1
Real-time Multivariate MJO series2	RMM2
Southern Oscillation Index	SOI
Tropical Northern Atlantic Index	TNA
Tropical Southern Atlantic Index	TSA
Western Hemisphere Warm Pool	WHWP

Table 3. Pearson correlation coefficients between the total annual rainfall series at Abu Dhabi Int'l Airport and the seasonal climate index series (3-months moving average).

Climate index	AMJ*	MJJ*	JJA*	JAS*	ASO	SON	OND	NDJ	DJF	JFM	FMA	MAM
AMO	-0.18	-0.12	-0.12	-0.18	-0.21	-0.21	-0.17	-0.13	-0.06	0.06	0.17	0.24
AO	-0.08	-0.21	-0.26	-0.02	-0.10	-0.02	-0.11	-0.04	-0.09	-0.08	-0.20	-0.33
GIAM	0.31	**0.43**	**0.44**	**0.51**	**0.48**	**0.56**	**0.57**	**0.63**	**0.61**	**0.57**	**0.62**	**0.59**
MEI	0.26	**0.43**	**0.52**	**0.53**	**0.54**	**0.54**	**0.56**	**0.57**	**0.59**	**0.59**	**0.57**	**0.54**
NAO	0.09	0.09	-0.02	0.18	0.03	0.04	-0.11	-0.06	-0.15	-0.07	-0.20	-0.21
NOI	-0.26	**-0.40**	**-0.55**	-0.36	**-0.42**	-0.30	**-0.42**	**-0.48**	**-0.54**	**-0.47**	**-0.47**	**-0.44**
ONI	0.39	**0.58**	**0.58**	**0.58**	**0.58**	**0.54**	**0.56**	**0.56**	**0.58**	**0.52**	**0.54**	**0.49**
PDO	0.10	0.21	0.30	**0.45**	**0.50**	**0.49**	0.36	0.27	0.28	0.34	**0.41**	**0.46**
PNA	0.07	0.15	0.09	-0.08	-0.16	-0.06	0.13	0.22	0.29	0.30	**0.43**	**0.43**
SOI	**-0.47**	**-0.47**	**-0.42**	**-0.44**	**-0.47**	**-0.50**	**-0.54**	**-0.53**	**-0.54**	**-0.51**	**-0.46**	-0.24
TNA	-0.11	-0.06	-0.06	-0.09	-0.08	-0.04	0.01	0.07	0.18	0.31	**0.39**	**0.43**
TSA	-0.16	-0.13	-0.22	-0.31	-0.32	-0.21	-0.12	-0.03	0.07	0.11	0.10	0.06
WHWP	0.01	0.08	0.08	0.12	0.12	0.16	0.22	0.35	**0.48**	**0.53**	**0.55**	**0.56**
DMI	0.12	0.16	0.18	0.26	0.34	**0.37**	**0.41**	**0.43**	0.34	0.03	-0.22	-0.33
MOI	0.05	-0.25	**-0.56**	-0.32	-0.21	0.18	-0.03	-0.13	-0.17	0.00	0.09	0.03
EA	-0.22	-0.30	-0.32	-0.24	-0.01	0.09	0.18	0.28	0.18	0.07	0.00	-0.02
RMM1	-0.22	-0.05	0.20	0.34	0.23	0.22	-0.04	-0.07	**-0.41**	-0.36	**-0.47**	0.12
RMM2	0.15	0.11	-0.14	-0.06	-0.30	-0.09	-0.16	-0.03	0.10	-0.05	-0.08	-0.35
MJO (amp)	0.30	0.19	0.25	0.15	-0.07	-0.08	0.01	0.15	-0.07	0.07	0.17	0.25

*Denotes a season occurring before the current hydrological year.
Bold values denote correlations statistically significant at $p<0.05$.

Table 4. AIC for the stationary case and for the nonstationary cases. For the nonstationary cases, the results presented are those obtained for the model leading to the best fit according to AIC.

Variable	Covariate	Abu Dhabi		Dubai		Ras Al Khaimah	
		AIC	Model	AIC	Model	AIC	Model
Total rainfall (mm)	Stationary	301.6	G0	412.9	G0	346.2	G0
	Time	302.6	G1	414.6	G1	347.4	G1
	ONI(JJA*)	297.8	G1	411.8	G1	**345.9**	G1
	NOI(JJA*)	298.9	G1	**411.4**	G1	346.7	G1
	Time - ONI(JJA*)	299.1	G(1-1)	413.4	G(1-1)	346.9	G(1-1)
	Time - NOI(JJA*)	300.6	G(1-1)	412.8	G(1-1)	347.8	G(1-1)
	ONI(JJA*) - NOI(JJA*)	**298.9**	G(1-1)	412.9	G(1-1)	347.8	G(1-1)
Total rainfall (mm)	Stationary	311.5	GEV00	406.0	GEV00	415.5	GEV00
	Time	311.1	GEV01	407.3	GEV10	416.7	GEV10
	ONI(JJA*)	304.3	GEV21	**404.0**	GEV20	412.1	GEV20
	NOI(JJA*)	307.9	GEV21	406.2	GEV01	411.1	GEV21
	Time - ONI(JJA*)	306.2	GEV(1-2, 2-1)	404.3	GEV(1-2, 0-0)	413.1	GEV(1-2, 0-0)
	Time - NOI(JJA*)	308.9	GEV(1-1, 1-1)	408.5	GEV(1-2, 0-0)	412.4	GEV(1-2, 0-1)
	ONI(JJA*) - NOI(JJA*)	**303.0**	GEV(2-1, 0-0)	404.8	GEV(2-1, 0-0)	**410.5**	GEV(1-2, 0-1)
Maximum rainfall (mm)	Stationary	253.9	GEV00	328.0	GEV00	314.8	GEV00
	Time	254.9	GEV01	328.7	GEV20	316.7	GEV01
	ONI(JJA*)	251.0	GEV21	328.1	GEV10	308.6	GEV21
	NOI(JJA*)	253.2	GEV10	324.8	GEV21	308.5	GEV20
	Time - ONI(JJA*)	251.8	GEV(2-2, 0-0)	325.5	GEV(2-2, 0-0)	310.6	GEV(1-2, 0-0)
	Time - NOI(JJA*)	252.6	GEV(1-0, 0-1)	326.8	GEV(1-2, 0-1)	310.3	GEV(1-2, 0-0)
	ONI(JJA*) - NOI(JJA*)	**249.9**	GEV(2-1, 0-0)	**323.6**	GEV(2-2, 0-0)	**301.8**	GEV(1-2, 1-1)

Bold values denote the best statistics for each station and rainfall variable.

Figures

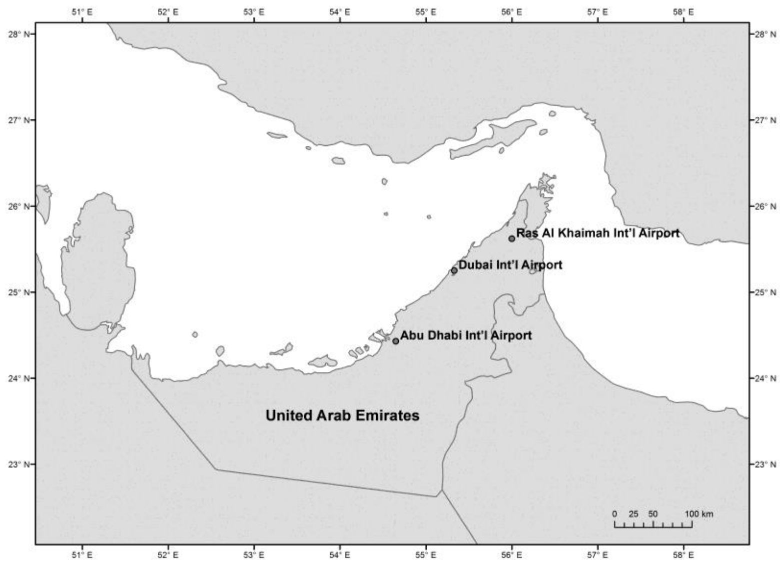

Figure 1. Spatial distribution of the meteorological stations.

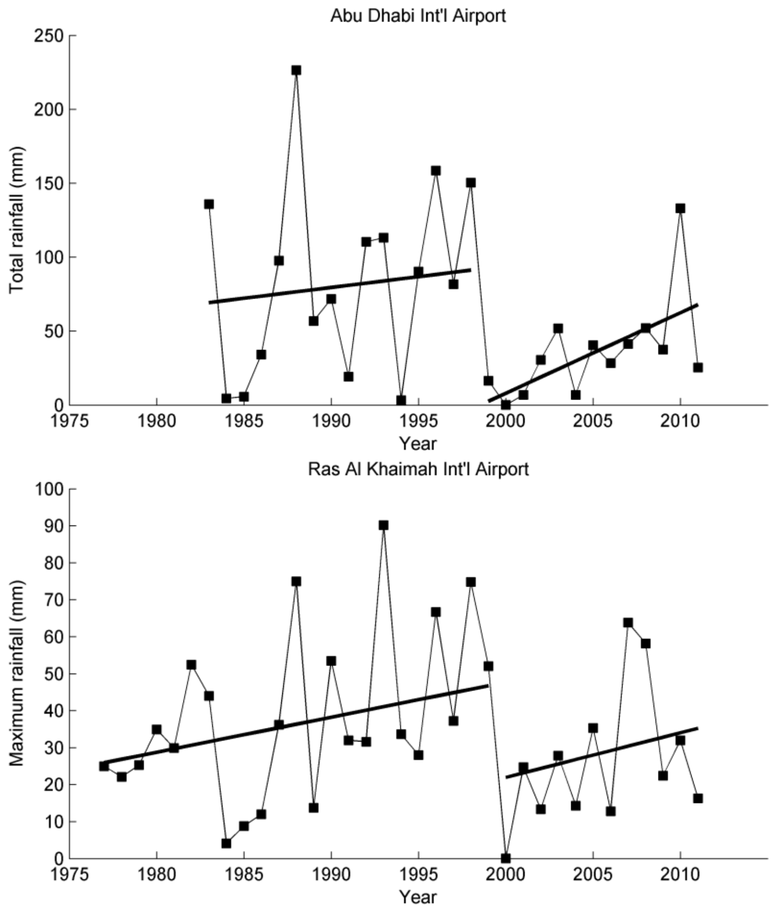

Figure 2. Linear trends for the total annual rainfall at Abu Dhabi airport and for the annual maximum rainfall at Ras Al Khaimah airport.

a)

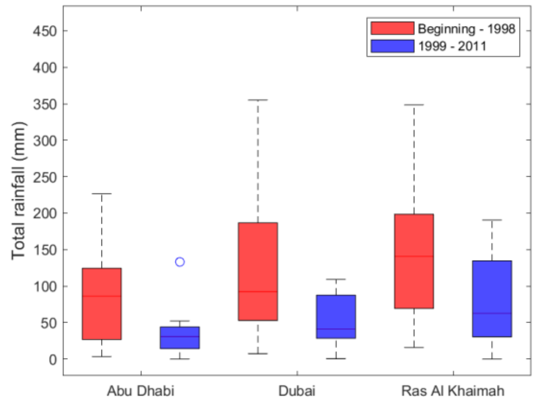

b)

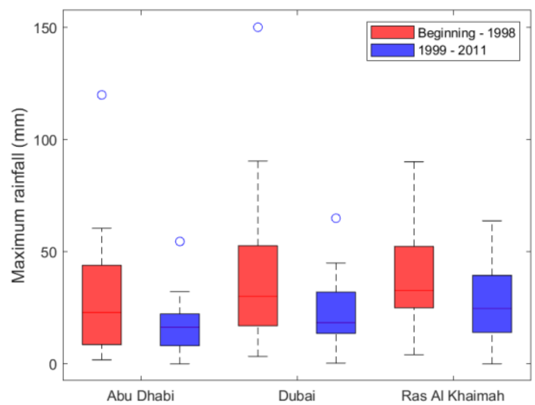

Figure 3. Box plots of a) total annual rainfalls and b) annual maximum rainfalls before and after the change point.

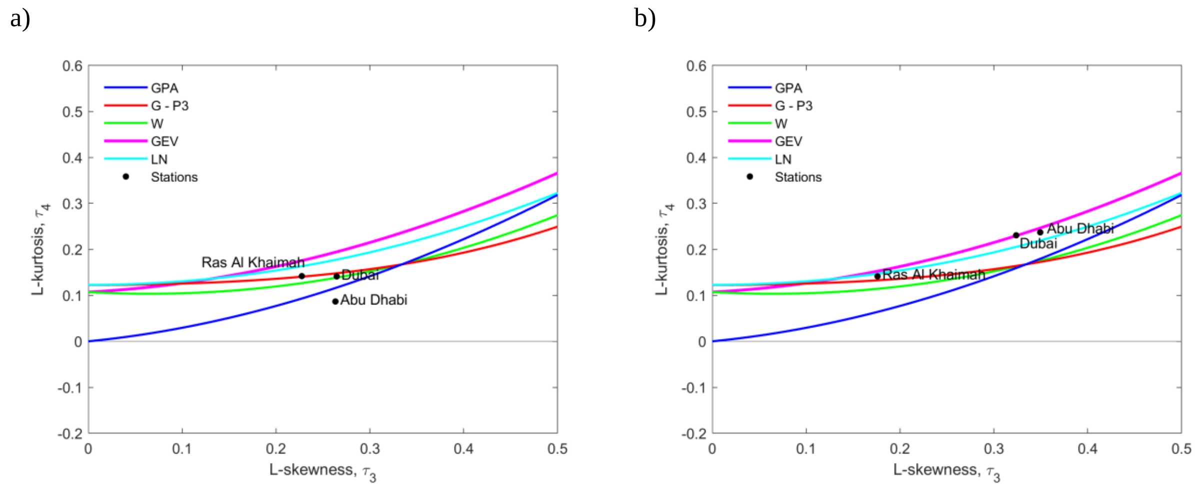

Figure 4. L-moment ratio diagram for the total annual rainfall (a) and the annual maximum rainfalls (b) at the rainfall stations.

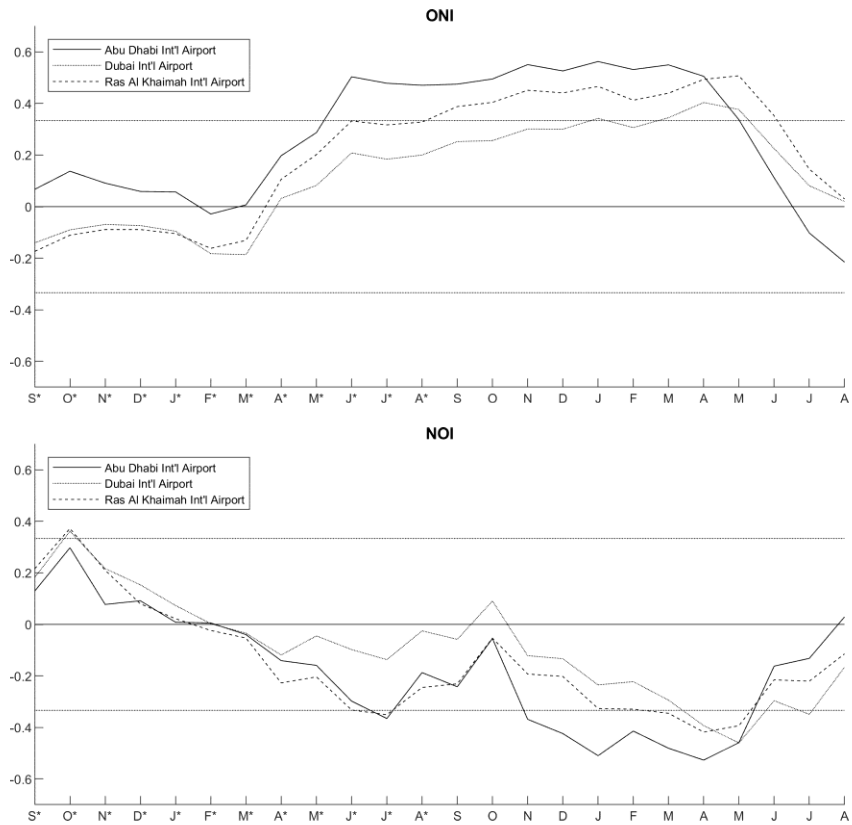

Figure 5. Pearson correlation coefficients between the annual total rainfall at each rainfall station and the 3-month moving average of the climate indices ONI and NOI. The central month used to compute the 3-month average is given on the x-axis. * denotes an index happening during the previous hydrological year. Horizontal dotted lines indicate significant correlations at 5%.

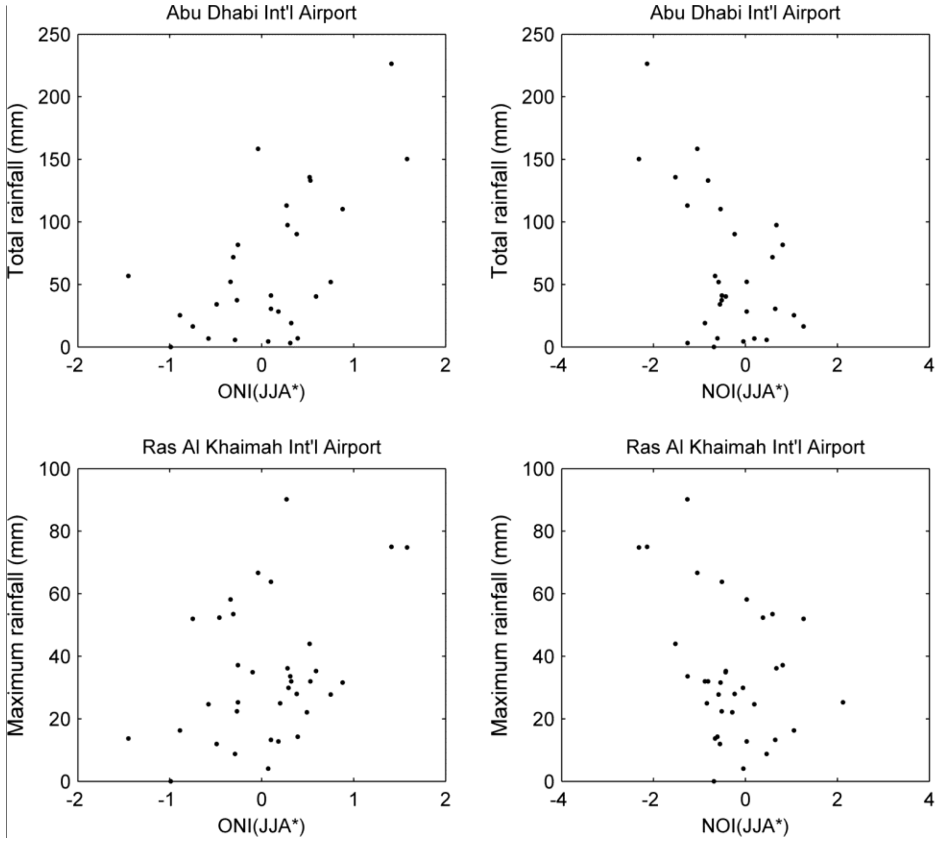

Figure 6. Scatter plots of total annual rainfalls for Abu Dhabi and annual maximum rainfalls for Ras Al Khaimah versus each selected covariates.

a) b)

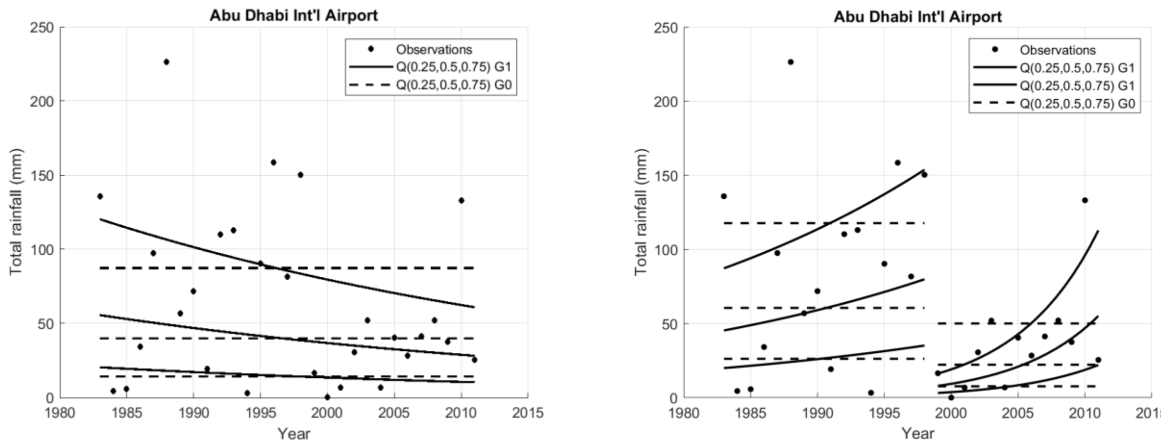

Figure 7. Quantiles corresponding to nonexceedance probabilities p = 0.25, 0.5 and 0.75 for the total annual rainfall at Abu Dhabi as a function of time for the nonstationary model including time as a covariate. In (a), the nonstationary model is fit to the whole sample where the model leading to the best fit is illustrated. In (b), two nonstationary models are fitted separately on the subsamples where the model leading to the best fit is illustrated in each subsample.

a) b)

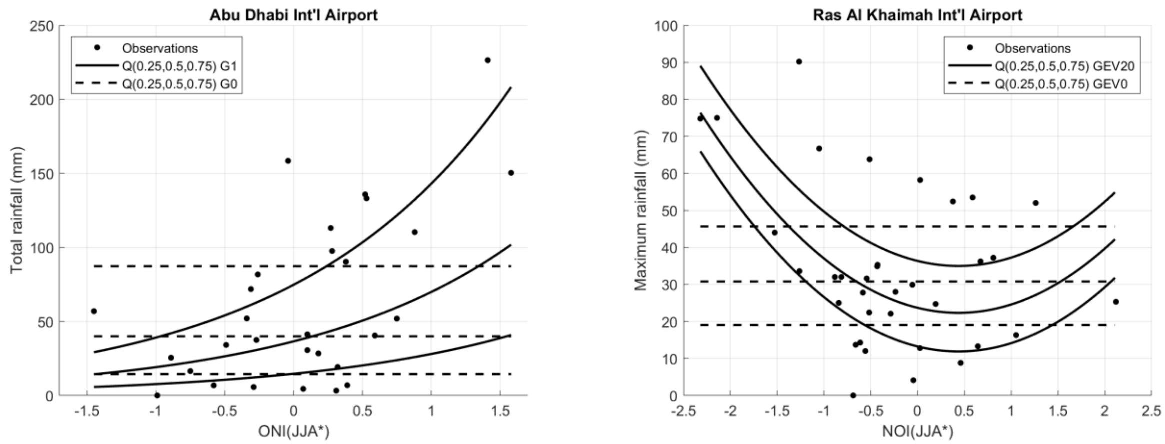

Figure 8. Quantiles corresponding to nonexceedance probabilities p = 0.25, 0.5 and 0.75 for the total annual rainfall at Abu Dhabi as a function of ONI(JJA*) for the nonstationary model including ONI(JJA*) as a covariate and the annual maximum rainfall at Ras Al Khaimah as a function of NOI(JJA*) for the nonstationary model including NOI(JJA*) as a covariate. In each case, the model leading to the best fit is illustrated.

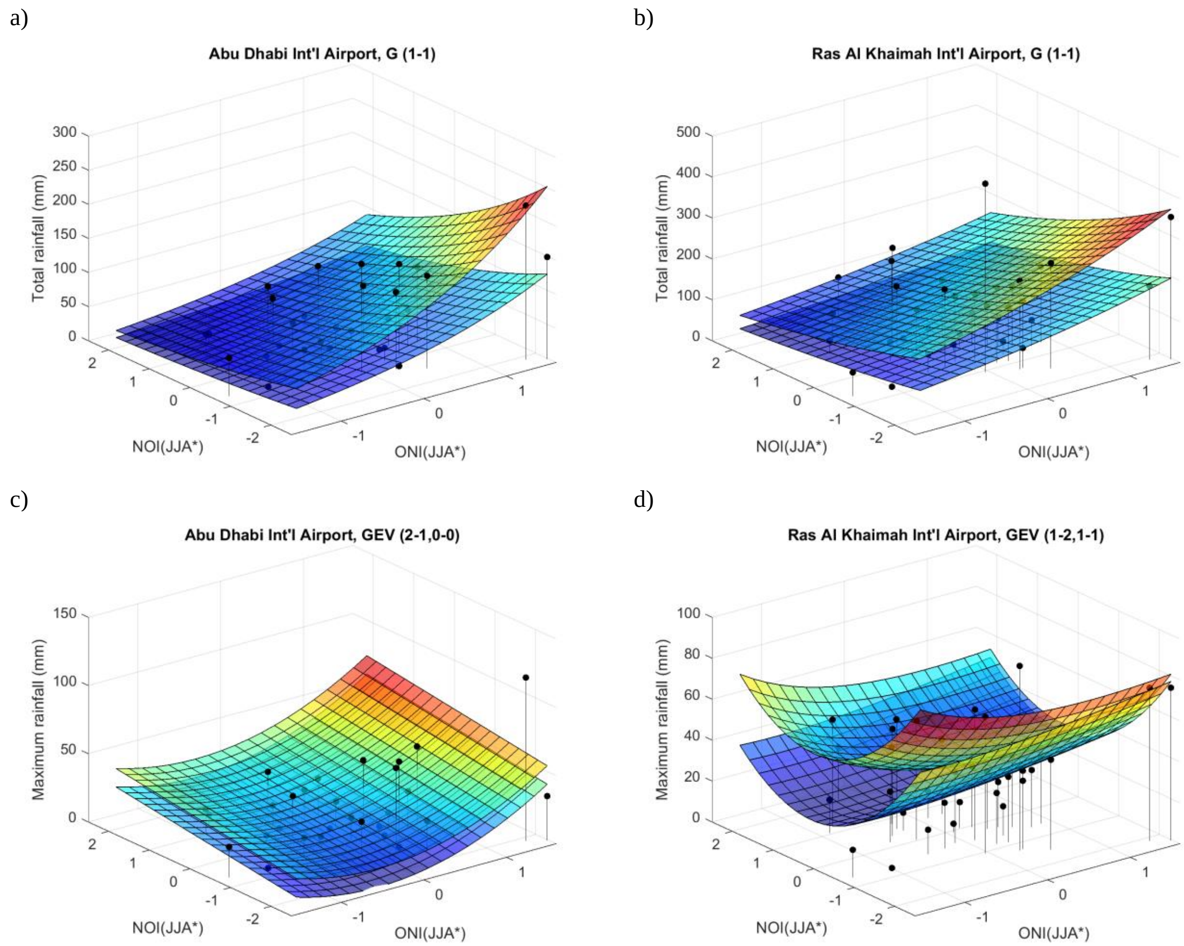

Figure 9. Quantiles corresponding to nonexceedance probabilities p = 0.5 and 0.75 for the total and maximum annual rainfall at Abu Dhabi (a and c) and Ras Al Khaimah (b and d) as a function of ONI(JJA*) and NOI(JJA*) for the nonstationary model including ONI(JJA*) and NOI(JJA*) as a covariates. In each case, the model leading to the best fit is illustrated.

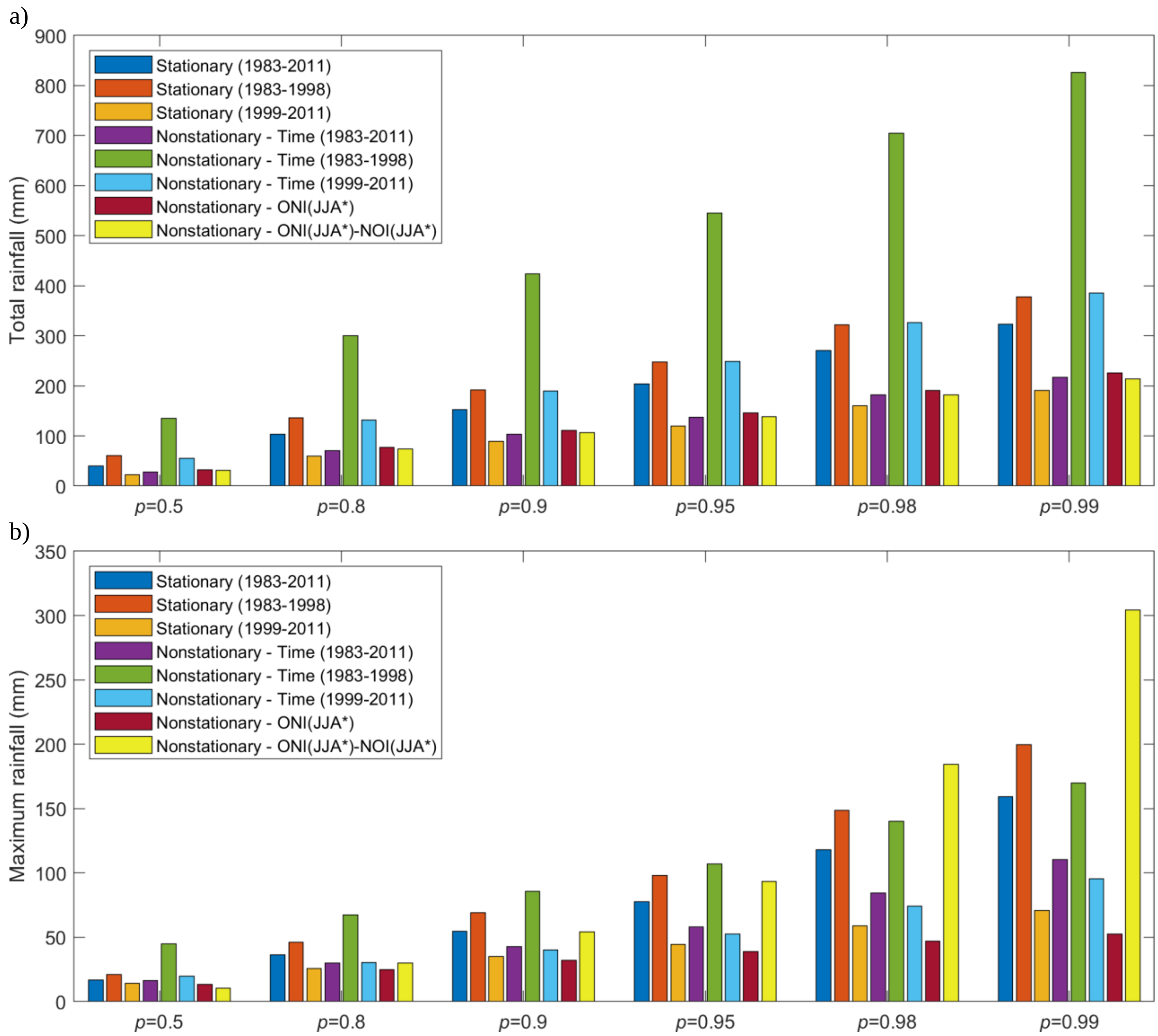

Figure 10. Quantiles for the annual total rainfall (a) and the maximum annual rainfall (b) obtained with the stationary model and the nonstationary model with the time, one climate index and two climate indices as covariates at the Abu Dhabi station. The stationary model and the nonstationary model with time were applied to the whole time series (1983-2011), and to the subseries for the periods 1983-1998 and 1999-2011. Predicted quantiles correspond in each case to the condition at the year 2012.

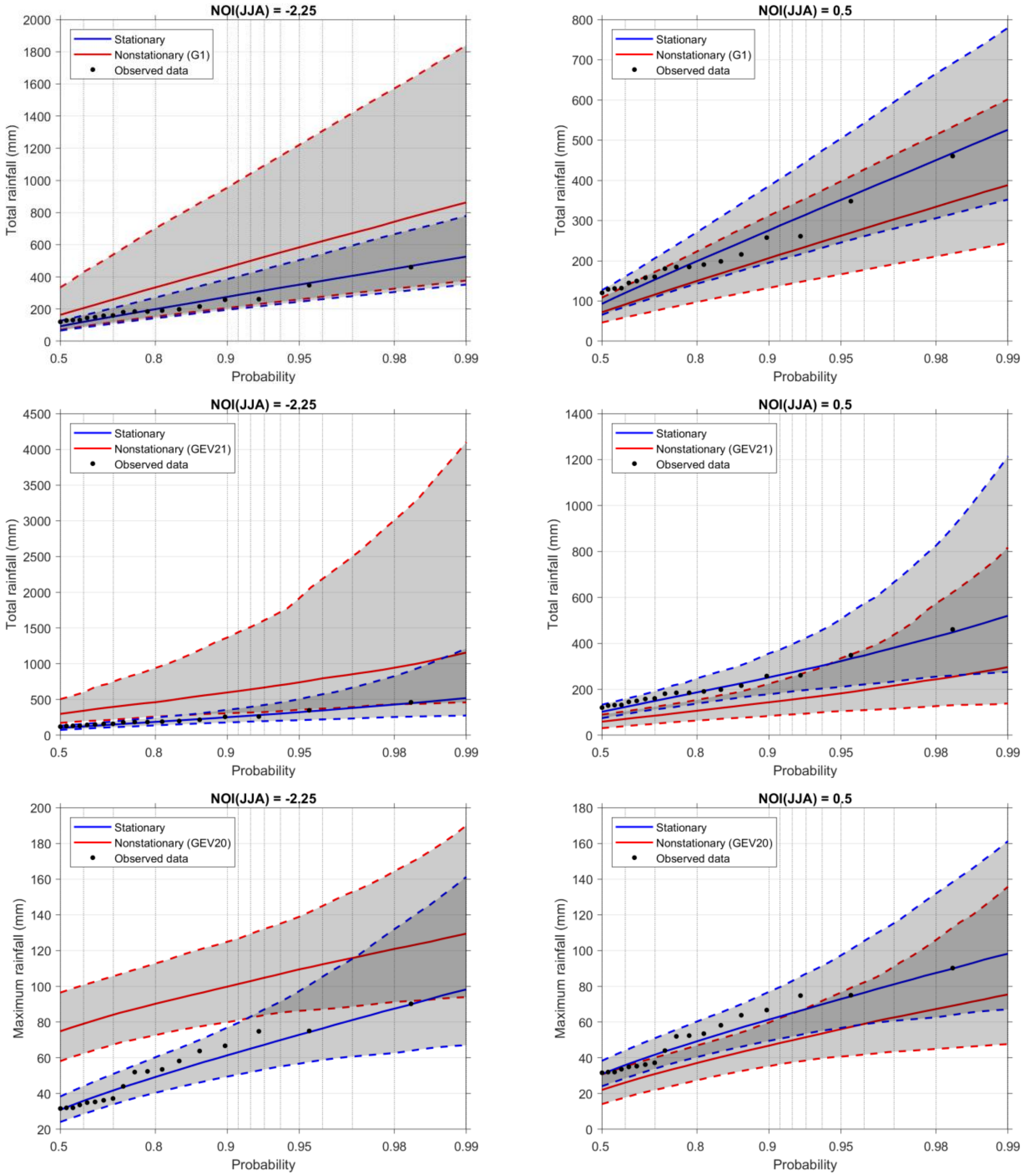

Figure 11. Graphs of quantiles versus exceedance probabilities comparing the stationary model and the nonstationary model with NOI(JJA*) as covariate. Cases for the total and maximum annual rainfalls at Ras Al Khaimah are illustrated for values of NOI(JJA*) equal to -2.25 and 0.5. 95% bootstrap confidence intervals are specified for each curve.

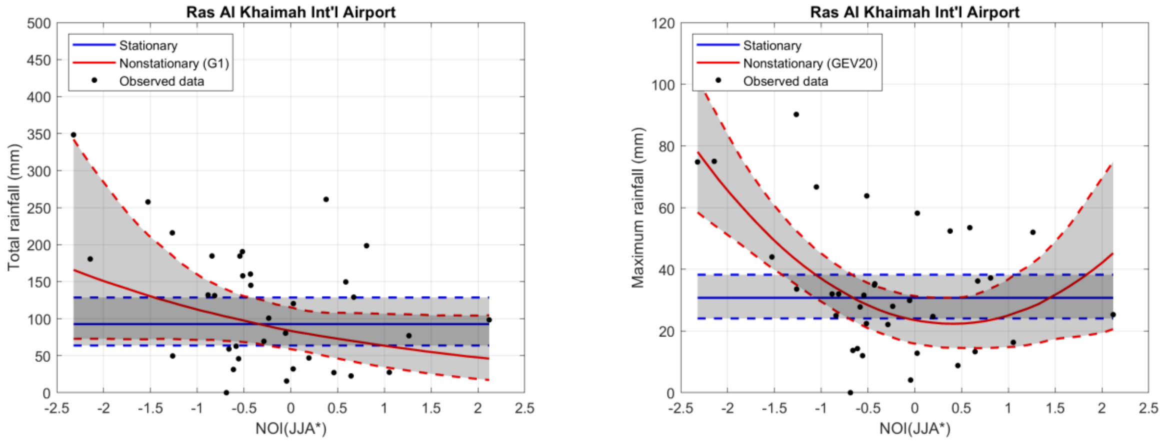

Figure 12. Graphs of quantiles versus the covariate values comparing the stationary model and the nonstationary model with NOI(JJA*) as covariate. Cases for the total and maximum annual rainfalls at Ras Al Khaimah are illustrated for an exceedance probability of p = 0.5. 95% bootstrap confidence intervals are specified for each curve.

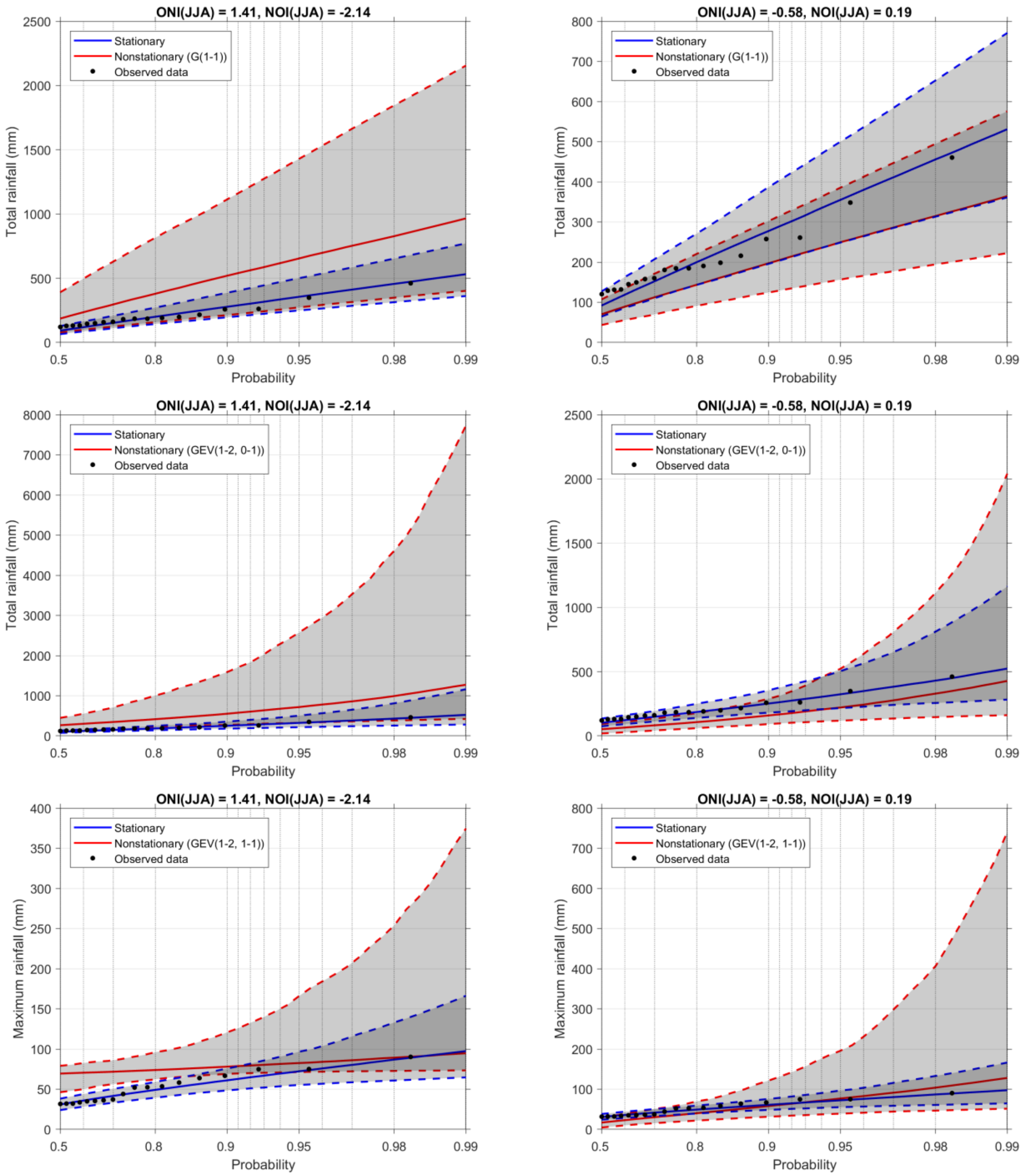

Figure 13. Graphs of quantiles versus exceedance probabilities comparing the stationary model and the nonstationary model with ONI(JJA*) and NOI(JJA*) as covariates. Cases for the total and maximum annual rainfalls at Ras Al Khaimah are illustrated for values of ONI(JJA*) and NOI(JJA*) equal to respectively 1.41 and -2.14, and respectively to -0.58 and 0.19. 95% bootstrap confidence intervals are specified for each curve.